Concrete slabs reinforced with GFRP materials

Experimental and numerical study

Filipe Silva Rocha
filipe.srocha14@gmail.com
IST, Instituto Superior Técnico, Portugal

Abstract: Fibre reinforced polymers (FRPs), more specifically glass-FRP (GFRP) bars, are an interesting alternative to be used as internal reinforcement in concrete structural elements, combining the advantage of being non-corrodible with reduced self-weight and very high strength. This study presents the results of concrete slabs reinforced with GFRP bars when subjected to concentrated loads, typically adopted for designing bridge decks. The slabs' design was based on a numerical model to evaluate the design internal forces and simulate the steps of the experimental study. Two flexural tests were performed, by loading real scale concrete slab prototypes internally reinforced with GFRP bars and angle GFRP profiles along the perimeter. In each experimental test, the prototypes mechanical behaviour was recorded during the loading sequence, namely the load-deflection curves, tension-extension curves, concrete crack patterns, and ultimate resistance and failure modes. These results are discussed and compared with the numerical predictions. Based on the two preformed tests and numerical investigations it is possible to confirm that reinforced concrete slabs can be designed using GFRP bars, in view of the excellent in service behaviour attained and failure loads reported, about two times higher than the required standard design loads.

Keywords: Reinforced concrete, glass fibre reinforced polymers (GFRP), structural behaviour, experimental study.

1 Introduction

In recent years there has been a significant increase in the cost of maintaining and repairing concrete structures reinforced with steel bars. Interventions in these structures are motivated by problems related to the following aspects: i) errors or deficiencies in various phases of the structures' life (design, execution, exploration or maintenance); ii) aggressive actions (physical, chemical or biological) and iii) changes in the use of the structure when compared to that was considered in the original design. These aspects are associated with a number of pathologies which may compromise correct its functioning and structural safety of [1]; corrosion of the internal steel reinforcement is one of the most frequent. In this context, fibre reinforced polymer (FRP) materials, originally developed for aerospace and naval applications, emerged as an alternative to traditional construction materials. FRPs have a high versatility as they can be composed of various types of fibre reinforcement and/or polymeric matrices, which translates into a wide range of FRPs on the market. With regard to the type of fibre reinforcements, carbon, glass and aramid fibres are the most common ones, originating CFRP (*"Carbon Fibre Reinforced Polymer"),* GFRP *("Glass Fibre Reinforced Polymer"*), AFRP, (*"Aramid Fibre Reinforced Polymer),* respectively. The main role of the fibres is related to the mechanical response of the material (strength and stiffness). The polymeric matrix is mainly constituted by resin, to which filling materials *(filler)* and other additives can be added; its main role is to ensure the transmission of forces between fibres and provide mechanical and chemical protection [2] against aggressive agents. The resins can be divided into two main types: thermoset and thermoplastic. Thermoset are the most common ones in FRP for civil engineering applications and include polyester, vinylester and epoxy [3].

2 Description of the experimental programme

The present work is based on a real project, and the tests were performed on full scale concrete slabs. The slabs specimens were designed based on the recommendations provided by CNR-DT203-2007 [4] and ACI 440.1R-15 [5]. Regarding the safety checks,

detailed information is provided in the main document of current Master's dissertation.

2.1. Objectives, test series and materials

One of the main problems of concrete slabs reinforced with steel bars is their durability when subjected to harsh environments; in this context, the use of GFRP bars as internal reinforcement of concrete slabs may be a very effective solution to mitigate the above mentioned vulnerability. First of all, there is the need to prove that the slabs reinforced with GFRP bars are a viable solution, namely in terms of their structural behaviour under service load combinations and up to failure.

The main objective of present study is to provide a better understanding of the short-term behaviour of concrete slabs reinforced with GFRP bars when loaded up to failure. An experimental program was carried out, including, at an early stage, the design and manufacture of the slabs and, subsequently, material characterization tests and bending tests of slabs at room temperature.

2.2. Specimens geometry and preparation

The geometry of the slabs were defined based on the requirement of a real project, therefore the tests were performed on real scale of specimens. Thus, the design followed the regulatory provisions used in the implementation project, in particular for the definition of loads and combinations of actions. Regarding the safety verifications, the provisions presented in the guidelines for the design of FRP-reinforced concrete structures were considered. The commercial *software* SAP2000® [6] was used to obtain both the design bending moment and shear force.

Regard to the geometry and boundary conditions of the slabs, simply supported rectangular panels with a length of 2.05 m and a width of 1.52m wide were used, its thickness was 0.17 m (**Figure 1**).

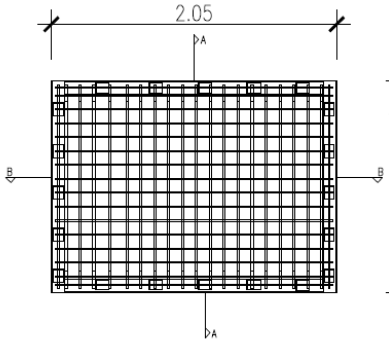

Figure 1 - Dimensions of the slabs ([m] not in scale).

The materials considered for the manufacture of the slab are:

- Concrete C35/45 XC3(P) Cl0,2 D_{max} 12 S3 (NP EN 206-1:2007 [7]);
- GFRP bars with diameters of 16 mm, 10 mm and 6 mm;
- Angle ("L") GFRP profiles.

The loading that was considered for the design was the self-weight of the slab, and, as it is a study focused on the scope of bridge decks, the types of loadings characteristic of these structures, in particular, two concentrated loads simulating two wheels (i.e. 1 axis) of the "design vehicle". Therefore, for the structural verification of concrete slabs, the FE model showed in **Figure 2** was used, which simulated the wheels of the vehicle.

The design bending moment was obtained using a FE model of the simply supported slabs with an approximate span of 1.42 m (cylindrical bending) (**Figure 2**). In addition to the permanent load, the slab was subject to two concentrated loads distanced 1.50 m (this is the position of the loads that lead to the maximum bending moment).

The concrete used in its production was a C35/45 ready-mixed concrete supplied by Unibetão.

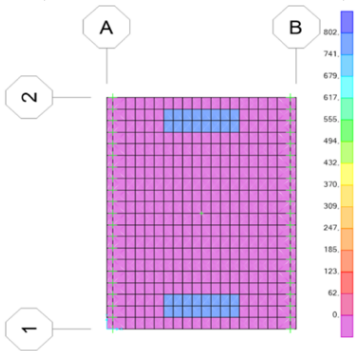

Figure 2 – FE model of the slab with two concentred loads.

Table 1 - Dimensions of the main reinforcement (lower)

Design bending moments and reinforcement adopted		
A_f inf. [cm²/m]	20,11	Φ16 // 0,10
A_f sup. [cm²/m]	2,83	Φ6 // 0,10
A_f const. [cm²/m]	2,83	Φ6 // 0,10
M_{cr}[kNm]	15,80	
M_{freq}[kNm]	15,40	
M_{Ed} [kNm]	57,7	
M_{Rd} [kN.m/m]	95,72	

The main lower reinforcement consisted of 16 mm bars spaced of 10 cm; **Figure *3*** summarizes the final design solution with GFRP rebars.

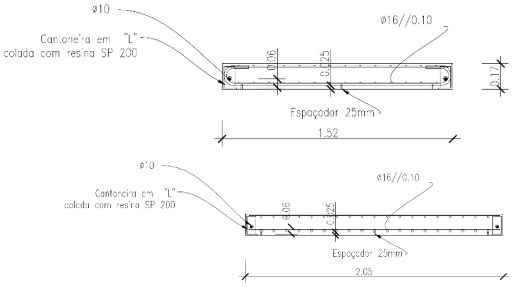

Figure 3 - Final solution of the slabs (Dimensions in meters; not in scale).

2.3. Test setup, instrumentation and procedure

The loading frame consisted of two columns and a beam. One of the columns consisted of a HEB 400 profile (steel S355), whereas the other was a HEB 500 profile. The beam, with a span of 3.6 m, was also a HEB 400 profile (steel S355), connected to the columns through 8 M24 bolts (class 8.8) in each joint.

To apply and measure the load applied, a hydraulic jack and a load cell (both with a capacity of 1000 kN) were used, respectively. The columns were fixed to the laboratory floor slab through two high resistance bars (diameter 36 mm), pre-tensioned to a force of approximately 500 kN/bar.

The slabs were supported on 4 concrete blocks (square cross section of 50 cm; with 87 cm of height) allowing a direct observation of their lower surface, namely of the crack development and failure mode. These concrete blocks were levelled with plaster. On top of these blocks, HEB 220 profiles were positioned to simulate continuous support along two edges of the slabs. Between these profiles and the slabs, a continuous membrane of neoprene (10 mm thick), was placed in order to fill possible imperfections/gaps between the slabs and the HEB 220 profiles. **Figure *5*** shows the test setup adopted.

The positioning of the strain gauges in the GFRP rebars and angle profiles (similar in both slabs) is showed in **Figure 4**.

The vertical displacements of the slab during the tests were measured using displacement transducers, either on the top face of the slab (one in each corner of the slab) or on the bottom face (in the alignment of the applied loads and at midspan; this positioning was the same on both slabs).

The displacement transducers on top surface of the slab were positioned on the corners in order to the deformability of the neoprene.

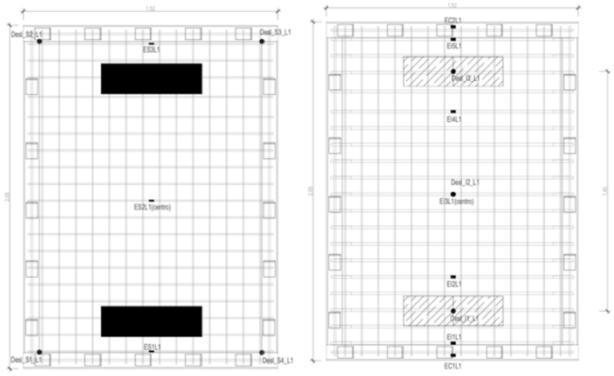

Figure 4 - Instrumentation of slab 1 (similar in slab 2).

It is important to note that during the experimental campaign there was a change in loading mode from slab 1 to slab 2, from the axle of the vehicle type to a “half-vain” concentrated load. This change aimed at studying of GFRP-reinforced concrete slabs under a different loading configuration, thus contributing for a better understanding of their structural response.

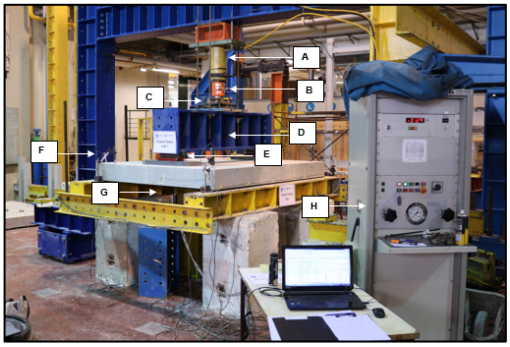

Figure 5 - Test scheme used for the bending tests. A- Hydraulic jack; B-load cell; C-spherical hinge; D-load transmission beam (HEB400); F,G – displacement transducers; H-hydraulic pressure unit.

3 Results and discussion

The objective of this section is to present and discuss the results of the bending tests on the slabs. It is worth remembering that these tests have the main objective of verifying the feasibility of developing concrete structural elements reinforced with GFRP bars.

The maximum bending moment (m11) obtained in the FE model for the ULS load combination was 59.7 kN.m/m for slab 1. The value of m11 for a loading scenario that considers only the self-weight of the structure was analysed, obtaining the values illustrated in **Figure *6***a. When comparing the m11 values presented in this figure, it is concluded that the bending moment due to the self-weight is less than 5% of the ULS design bending moment. For this reason, in the results presented in the current section, the contribution of the self-weight was neglected; this assumption was also considered for slab 2, as the magnitude of the bending moment due to the self-weight when compared to the ULS design value was similar to that of slab 1.

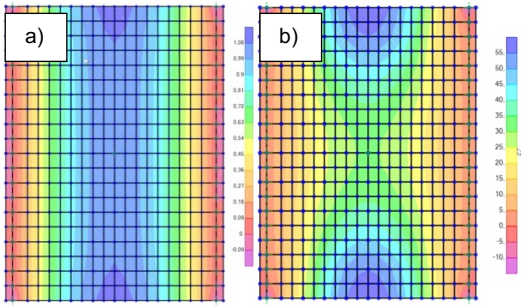

Figure 6 - Bending Moment m11 in slab 1: a) due to self-weight; b) for the ULS load combination.

3.1. Load vs. displacement diagram

Slab 1

In **Figure 7** are illustrated the different load-displacement diagrams obtained in slab 1 and it is possible to identify a branch with similar development from the beginning of the test to approximately 80/90 kN (total load value applied). This branch corresponds to the elastic phase of the slab, presenting higher stiffness values that were significantly reduced due to cracking from loads higher than 80/90 kN.

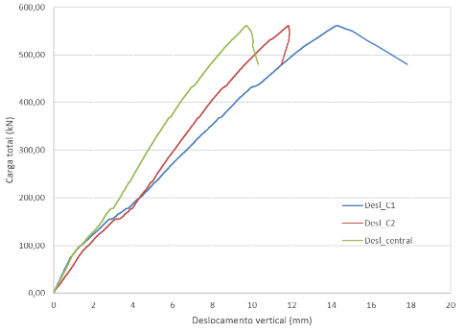

Figure 7 - Load-displacement response of slab 1

In **Figure 7** it is also observed that the rupture occurs for a total load of about 557 kN (i.e. 278.5 kN at each loading point on the slab - assuming perfect symmetry on the loads' distribution) – this value is about twice the design load (1.5x100 kN/wheel).

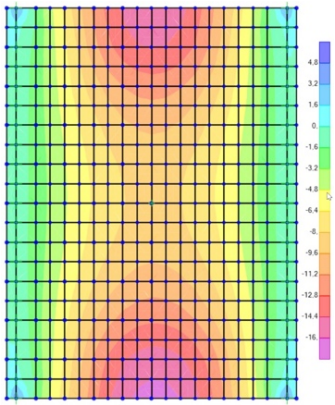

Figure 8 - M11 for a total load of 85 kN (42.5 kN in each loading point) for slab 1 corresponding to the beginning of crack development

As expected, and according to the results from previous studies [8], the slabs reinforced with GFRP bars present, after cracking, an approximately constant stiffness up to failure. It is important to note that the small reductions in the load values that were observed can be related to the following two phenomena: i) when a new crack opens and/or ii) when the boundary conditions changed, i.e. the initial gaps/clearances between the slab and the supporting structure were eliminated.

From plots showed in **Figure *9***, and as observed during the experimental campaign, it can be concluded that support conditions were not exactly the ones assumed in the design – an unsupported length of about 40/50 cm was observed along the border close to the

corner S4 – this "cantilever" length was maintained during the entire test. This may justify an asymmetry on the load distribution and might have influence on the failure mode obtained.

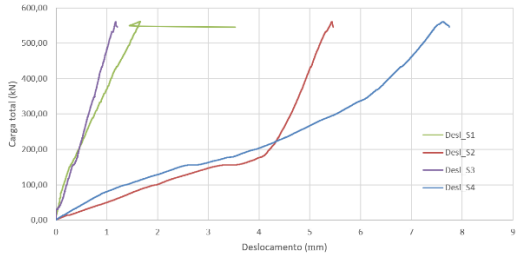

Figure 9 - Load-displacement diagrams of the corners of slab 1, measured on the top surface.

The contribution of the GFRP angle profiles placed along the perimeter of the slab was not totally understood. They might have provided a local stiffness increase along the borders, therefore changing the way the loads were transferred throughout the slabs. This joint should be studied in the future with a more detailed model allowing for a better understanding on the way the forces are transmitted between the concrete and the GFRP angle profiles.

Slab 2

Figure 10 shows the load-displacement curves obtained in the slab 2.

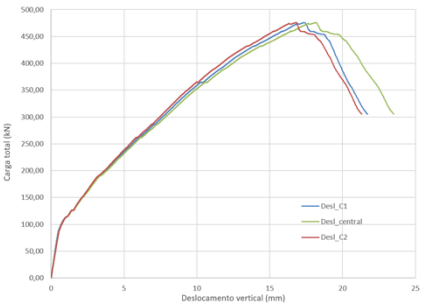

Figure 10 - Load-displacement diagrams along the midspan section of slab 2.

Due to the change in the slopes of the three curves that occurred about 80/90 kN, it was possible to identify the beginning of the cracking. Similarly to what was done for slab 1, an EF model was developed in SAP2000® to confirm the estimation of the cracking load. **Figure 11** illustrates the m11 bending moment diagram obtained for a total applied load of 85 kN where it is possible to observe that the maximum moment due to this load is approximately equal to the cracking bending moment (17 kN.m/m) – this result confirms that the beginning of the cracking occurred within the range 80/90 kN (total load). For loads higher than this value, it was found a slight increase in the nonlinearity of the curve until the maximum load (475 kN) is reached, which is the typical behaviour of concrete elements reinforced with GFRP bars.

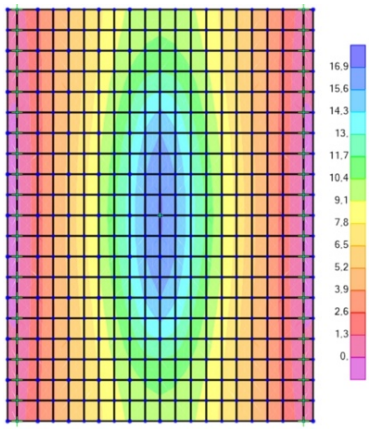

Figure 11 - m11 diagram for a total loading of 85kN (42.5kN in each loading point).

The displacements measured over the 4 corners in slab 2 are illustrated **Figure *12***; the significant differences between their developments indicates that the way the loads were transferred throughout the slab up to the supports should be different from that admitted in the design and in the FE model. This may explain the way and place where this slab failed; the rupture occurred closer to the corners Desl_S1 and Desl_S4 (see **Figure 1**), where smaller displacement were measured (i.e. to where more load may have been transmitted).

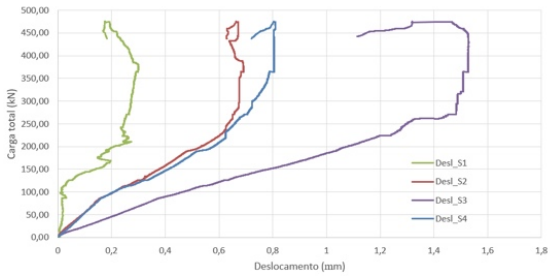

Figure 12 - Load-displacement curves of the corners of slab 2, measured on the top surface.

3.2. Extensions in the GFRP material

Slab 1

The **Figure 13** shows the extensions in the lower reinforcements (EI curves) and in the GFRP angle profiles (EC curves), measurements at the nearest and farthest ends of the slab failure point (respectively extensions EI1/EC1 and EI5/EC2 - see **Figure 1**. These curves can be divided into two phases: (i) the first corresponding to the elastic phase, that is, prior to the

beginning of the cracking (corresponding to a total load level within 80/90kN); (ii) the second phase corresponded to response in the cracked state.

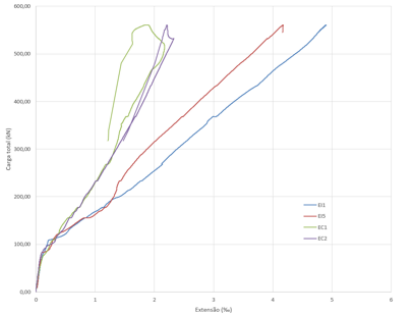

Figure 13 - Total load diagram - extensions in lower reinforcements (EI1 and EI5) and angle profiles (EC1 and EC2)

As can be observed in **Figure 13**, the maximum axial strain measured in the lower reinforcement (4.8‰ – EI1 extension gauge) is much lower than the material failure strain (20.2‰ – provided by the manufacturer). In the manufacturer's technical data sheets the tensile strength of the rebars is 1040 MPa; in the test of slab 1 the maximum tension on the lower reinforcement was 267 MPa, i.e. only about 26% of its tensile strength.

For the GFRP angle profiles, the tensile strength specified by the manufacturer is 482MPa; in the test of slab 1 test only a maximum tensile stress of 112 MPa was reached, i.e. only 23% of its resistance. Based on these results it is possible to conclude that the high tensile strength of both GFRP materials have not been efficiently explored; this is relatively common in concrete structures reinforced with these materials.

Regard to the connection between the GFRP angle profiles and the concrete, if there was a perfect connection between the two materials, the expected diagram of extensions would be the one showed in **Figure 14**. However, by analysing **Figure 13**, it can be concluded that this connection is not perfect; in fact, excluding some oscillations of the readings in the initial phase of the test (for reduced load levels), it is observed that for the same load level the tensile strains in the angle profiles are significantly lower than those of the lower rebars, indicating that the extensions are discontinuous in the concrete-GFRP angle profile interface. Still, the stresses mobilized in the angle profiles are significant (maximum of 112 MPa), showing that the connection system was effective, allowing them to contribute partially to the overall response of the slab.

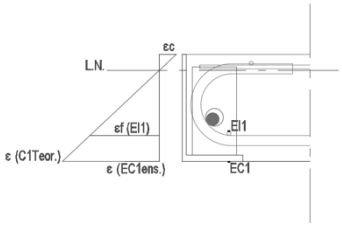

Figure 14 - Qualitative strain diagram assuming a perfect connection between the concrete and the GFRP angle profiles

Slab 2

Figure 15 shows the curves of the strains measured in the lower rebars (EI curves) and in the angle profiles (EC curves), measured at the nearest and farthest ends from the slab's failure point. When analyzing the development of the curves illustrated in this figure it is possible to conclude that, globally, it is similar to what was observed in slab 1; thus, two distinct phases are distinguished: (i) elastic phase - from the beginning of the test to the beginning of the concrete cracking (around 80/90 kN); (ii) elastic cracked phase – where the strain values increased significantly until the maximum load is reached, presenting an overall behaviour that can be assumed to be close to linear.

Regarding the strain values, and similar to slab 1, these indicate that the stress levels reached in the GFRP materials are relatively low – 179 MPa in the case of the lower GFRP rebars (17% of their tensile strength) and 61 MPa in GFRP angle profiles (about 10% of tensile strength).

Regard the comparison between the strain values of the internal reinforcements and of the angle profiles, it is observed that for the EI5/EC2 pair, the strains in the angle profiles are significantly lower than those in the lower reinforcement, showing again that the strain diagram is discontinuous in the concrete-angle profile interface – this result is in agreement with that obtained on slab 1 and shows that in this location the concrete-angle profile connection is very flexible. For the pair EI1/EC1, it is observed that the strain in the angle profile for all load levels (including the elastic phase of the slab response) is higher than the strain values in the rebars – this result, opposite the previous one, indicates that in this location the concrete- angle profile and failure modes.

connection may have been more effective. Due to the complexity of the phenomena involved in the behaviour

Experimental Results		Calculations with theoretical average strength for a C35/45 concrete		Calculations with average strength at 77 days of age	
Failure load [kN]	Failure mode	Failure load (bending) [kN]	Failure mode	Failure load (bending) [kN]	Failure mode
577,0	E.T./P	589,1	E.B.	614,9	E.B.

of this connection, and because this conclusion is supported by strain readings on only 2 strain gauges, it is recommended to carry out additional studies to provide a better understanding of structural efficiency of this connection system.

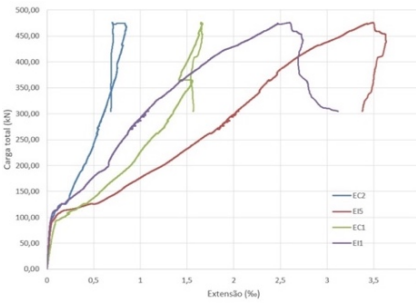

Figure 15 - Total load vs. strains diagrams for the GFRP rebars (EI1 and EI5) and GFRP angle profiles (EC1 and EC2) in Slab 2.

3.3. Failure loads, failure modes and comparisons with code's previsions

Slab 1

Figure *16* presents the crack pattern at the bottom surface after the test of slab test 1.

On this slab, cracking was also observed on the top surface. This non-expectable cracking may be related to the fact that the support conditions were not the most perfect, in particular because a considerable length of one of the edges of the slab was unsupported throughout the test.

The failure load value and failure mode obtained experimentally are indicated in

Table 2. In this table, the values of the predicted failure loads and the corresponding failure modes were also included in the design, in which two different values of concrete compressive strength: (i) the expected average value for a concrete class C35/45; and (ii) the experimental mean value obtained at the age of testing (77 days). By the analysis of

Table 2 it is possible to conclude that there are significant differences between the experimental results and the predictions, both in terms of the failure loads and failure modes. How can be observed **Figure *16***, punching shear failure was obtained in slab 1, which was not initially predicted on its design.

Table 2 - Experimental and predicted failure loads

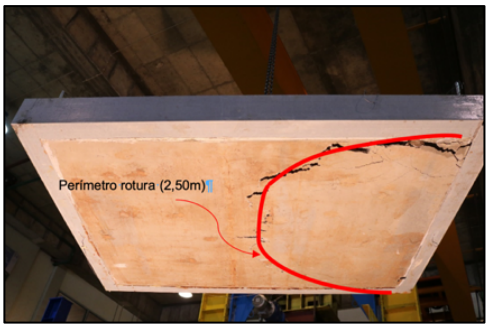

Figure 16 - Failure mode of slab 1.

Notes: E.T./P – Shear failure (punching shear); E.B. - concrete crushing;

Table *3* shows the maximum values of the bending moment obtained in the SAP2000 model® for the design loading (38.45 kN.m/m due to the total load of 200 kN = 2 × 100 kN/wheel; 57.70 kN.m/m associated with the increased value of the total load of 300 kN = 1.5 × 2 × 100 kN/wheel). To estimate the failure load based on the formulations of the design guidelines, it was assumed that the elastic response of the slab remained valid up to rupture, thus, for the design bending moment of M_{Rd} = 95.72 kN.m/m) a corresponding failure load of 498 kN was obtained. Using the value of the flexural strength calculated based on the average properties of the materials ($M_{ult\_bending}$ =139.02kN.m/m) the corresponding failure load would be 722 kN, which is much higher than that obtained in the experimental campaign (P_{ult_assay} = 560.5 kN). It is worth mentioning that in this analysis it is assumed that the elastic bending diagrams remained valid up to failure (which is a very simplistic approximation) and that the failure mode is characterized by concrete crushing (bending failure); as already mentioned, in the test punching shear failure was observed, which naturally explains the difference

between the predictions of the failure load (722 kN - associated to bending failure) and the experimental value (560.5 kN). Despite these differences between loads and expected failure modes, it is possible to observe in the **Table *3*** that the slab was able to withstand a maximum load 1.86 times higher than the design value.

It has been observed in the test that shear failure occurred and the respective perimeter of the rupture line (2.3 m – see **Figure *16***, with these data, more precise estimates/calculations of the failure load were performed. To this end, the formulations proposed in EC2 and CNR-DT-203-2006 were used to check safety to shear load of elements without specific reinforcement. **Table *3*** summarizes the maximum load estimates considering the design and average values of the material properties, as well as some of the main parameters involved in the calculations.

Table 3 - Summary of verification to shear failure

	EC2 (design)	EC2 (mean value)	CNR-DT 203 ($\rho_l = 0$)	CNR-DT 203 ($\rho_l = 0,007$)
f_{cd}; f_{cm} [MPa]	23,33	33,67	-	-
d [m]	0,137	0,137	0,137	0,137
U1 / b [m]	1,86	2,3 (	2,3	2,3
$V_{rd,c}$ [Mpa]	0,779	0,881	-	-
V_{min} [Mpa]	0,478	0,586	-	-
P_d ; P_{ult} [kN]	397,4	550,0	534,6	648,3
P_{exp} [kN]		560,5		

Slab 2

In **Figure *17*** the crack pattern obtained in bottom surface of slab 2 is showed, where it can be observed that it is quite different from that observed on slab 1 – naturally due to different positioning of loads. In this figure it is possible to observe that most cracks developped near one of the supported edges and along the larger dimensions of the slab. The location of this cracks is related to the failure mode obtained – as observed in **Figure *18***, the crack pattern observed after the test on slab 2 is quite different from that observed on slab 1 – naturally due to different positioning of loads. In this figure it is possible to observe that most cracks developed near one of the supported edges and along the larger dimensions of the slab. The location of these cracks is related to the different failure mode – as observed in **Figure *17***. Also, the curvature of the failure surface is greatly reduced.

Table 4 - Summary of the failure loads (Computed with design values and average materials properties)

M_{Vt} [kNm/m]	38,45	P_{Vt}[kN]	200	Coef. Seg.
M_{Ed} [kNm/m] (reference)	57,70	P_{Ed} [kN]	300	1,00
M_{Rd} [kNm/m]	95,72	P_{Rd} [kN]	498	1,66
$M_{ult\_bending}$ [kNm/m]	139,02	$P_{ult\_bending}$ [kN]	722	2,41
Punching shear failure		$P_{ult\_exp.}$[kN]	560,5	1,86

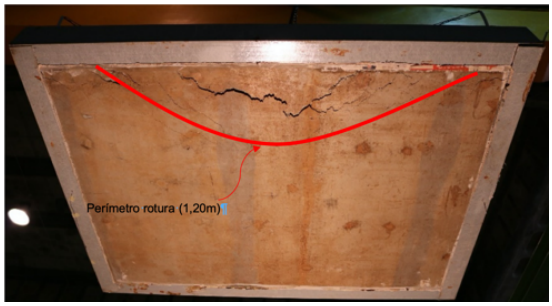

Figure 17 - Failure mode of slab 2.

Figure 18 - Side view of the failure mode in slab 2.

Table 5 - Summary of verification to shear failure

	EC2(design)	EC2 (mean value)	CNR-DT 203 ($\rho_l = 0$)	CNR-DT 203 ($\rho_l = 0,007$)
f_{cd}; f_{cm} [MPa]	23,33	33,67	-	-
d [m]	0,137	0,137	0,137	0,137
U1 / b [m]	3,66	2,05	2,05	2,05
$V_{rd,c}$ [Mpa]	0,794	0,881	-	-
V_{min} [Mpa]	0,478	0,574	-	-
P_d; P_{ult} [kN]	390,9	494,7	476,5	590,2
P_{ensaio} [kN]		**475,0**		

Considering the same simplifications assumed in slab 1, **Table 4** shows that the value of the design flexural strength calculated based on the average values of the material properties ($M_{ult\_bending}$ = 139.02 kN.m/m) corresponded to a failure load of 722 kN, which is much higher than the experimental value (P_{ult_exp} = 475 kN). In addition to all the approximations involved in calculation of this failure load, the great difference in the results is mainly associated with the fact that slab failed due to punching shear. Still, the slab was able to withstand a maximum load 1.58 times higher than the design value.

Table 6 - Summary of the main estimates for the maximum loads in slab 2.

M_{Vt} [kNm/m]	**41,10**	**P_{Vt}[kN]**	**200**	**Coef. Seg**
M_{Ed} [kNm/m] (reference)	62,54	**P_{Ed} [kN]**	300	1,00
M_{Rd} [kNm/m]	95,72	**P_{Rd} [kN]**	458,16	1,53
$M_{ult\_flexão}$[kNm/m]	139,02	**$P_{ult\_bendind}$ [kN]**	666,87	2,22
Punshing shear failure		**P_{ult_exp} [kN]**	475	1,58

It is worth mentioning that the formulations proposed in EC2 and CNR-DT-203-2006 for elements without specific shear reinforcement were used to estimate the failure load due to shear failure. As was made for slab 1, in the case of CNR formulation, the maximum load was estimated considering (ρ_l =0,007) or (ρ_l = 0), i.e. the taking into account the dowel effect of the of the longitudinal reinforcement or neglecting its contribution, respectively. **Table 6** summarizes the maximum load estimates considering the design and average values of the material properties, as well as some of the main parameters involved in the calculation.

4 Conclusions

The experimental campaign allowed to characterize the structural response of concrete slabs reinforced with GFRP rebars. The main objective of the experimental campaign was to evaluate the mechanical response of slabs when subjected to high static loadings. To this end, during the tests, the evolutions of the displacements and strains in the internal reinforcements and in angles profiles placed along the slabs edges were measured over the time. In the case of slab 1, the actual loading of an axle of the vehicle type, defined in RSA [9] was simulated increasing the load gradually until the slab ruptured. Punching shear failure was observed around one of the load application points, for a total load of 558 kN. This value corresponds to 1.86 times the required standard design load, showing the solution is suitable/safe to be used for bridge decks applications.

For slab 2, the loading configuration was changed to evaluate its structural behaviour of a similar slab when subjected to different loading forms (simulating a linear "knife" loading specified in the RSA). This change also led to the shear failure of the slab for a total load of 475 kN. Nevertheless, on slab 2 the experimental failure load was much higher than the required standard design load (1.58 times higher).

In general, based on the two preformed tests and numerical investigations it is possible to confirm that reinforced concrete slabs can be designed using GFRP bars, in view of the excellent in service behaviour attained and failure loads reported – this is an interesting alternative to conventional steel-reinforced concrete slabs, particularly when subjected aggressive environments that accelerate the corrosion phenomena on conventional steel reinforcement.

References

[1] S. Srinivasan, A. S. Silva, S. V Nanukuttan, and M. M. Salta, *DuratiNET Concrete Strucutres: Durability factors and requirements*. 2012.

[2] J. R. Correia, F. Branco, and J. Ferreira, "Utilização de perfis pultrudidos de fibra de vidro (GFRP) na construção," in *Construção 2004 - 2º Congresso Nacional da Construção – "Repensar a Construção"*, 2004.

[3] J. R. Correia, "A utilização de materiais plásticos reforçados com fibras (FRP) na reabilitação de construções," 2009, pp. 1–79.

[4] CNR, "Guide for the design and construction of concrete structures reinforced with fiber-reinforced polymer bars," *Cnr-Dt-203/2006*, no. June, p. 39, 2006.

[5] A. C. I. Committee, *Guide for the Design and Construction of Structural Concrete Reinforced with Fiber-Reinforced Polymer (FRP) Bars*. 2015.

[6] CSI (2016), "Computers and Structures Inc., SAP2000 versão 18.1.1." .

[7] LNEC, "Decreto-Lei nº235/83 - RSA: Regulamento de Segurança e acções," *Diário da República*. 1983.

[8] P. Santos, "Resistência ao fogo de lajes de betão armadas com varões em compósito de GFRP," 2016.

[9] Comité Europeu Para a Normalização, "NP EN 1992-1: Projecto de estruturas de betão. Regras gerais e regras para edifícios," p. 259, 2010.